Synergistic effect of PMIA nanofiber membrane with dual-oriented network structure and $Li_{0.5}Bi_{0.5}TiO_3$ nanofibers for high-performance lithium metal batteries

Zhaozhao Peng[a], Nanping Deng[a,*], Xiaofan Feng[a], Junbao Kang[a], Shuaishuai Wang[b], Tinglu Zheng[b], Bowen Cheng[a, c], and Weimin Kang[a,*]

[a] State Key Laboratory of Separation Membranes and Membrane Processes/National Center for International Joint Research on Separation Membranes, School of Textile Science and Engineering, Tiangong University, Tianjin 300387, PR China.

[b] Shandong Provincial Key Laboratory of Olefin Catalysis and Polymerization, Shandong Chambroad Holding Group Co., Ltd., Economic Development Zone of Boxing County, Binzhou 256500, China.

[c] School of Material Science and Engineering, Tiangong University, Tianjin 300387, PR China.

*Corresponding author. E-mail addresses: dengnanping@tiangong.edu.cn (N. P. Deng), kangweimin@tiangong.edu.cn (W. M. Kang).

1. Experimental section

1.1 Preparation of oriented PMIA nanofibers

In this method, the oriented PMIA nanofibers are obtained by adjusting the rotational speed of the receiving roller by electrospinning technology. In this method, the oriented PMIA nanofibers are obtained by adjusting the rotational speed of the receiving roller by electrospinning technology. The 15 g polyphenylbenzamide (PMIA) was dissolved in 10.7 g N, N-dimethylacetamide (DMAC), and stirred at room temperature until uniform and transparent. After the antifoaming treatment, electrospinning began. Process parameters: Spinning voltage is 30 kV, receiving distance is 15 cm, receiving roller speed is 2500 r/min, tilt Angle between pipette and receiving roller is 30°, natural extrusion under gravity conditions. The obtained high orientation PMIA nanofibers were dried at 50 ℃ for 24 h for use.

1.2 Preparation of LBTO nanofibers

In this experiment, LBTO nanofibers were prepared by the method of electrostatic dissolution and blowing. Using 4.85 g bismuth nitrate pentahydrate ($Bi(NO_3)_3 \cdot 5H_2O$), 1.02 g lithium acetate dihydrate ($C_2H_3O_2Li \cdot 2H_2O$), 3.4 g tetrabutyl titanate ($Ti(OC_4H_9)_4$) and 3.6 g polyvinylpyrrolidone (PVP, MW=1300000 g mol^{-1}) as raw materials, 26.4 g N, N-dimethylformamide (DMF) was prepared as solvent solution. The solution was stirred at room temperature for 12 hours and then treated with ultrasonic defoaming and transferred to an electrostatic dissolving and blowing device. The process parameters are as follows: spinning voltage is 40 kV, air injection rate is 0.05 MPa, receiving distance is 80 cm. The resulting nanofibers were dried at 50 ℃ for 12 h. Finally, the dried nanofibers were pre-oxidized at 200℃ for 1 h, and calcined in air at 650 ℃ for 2 h to obtain LBTO inorganic nanofibers.

1.3 Preparation of LBTO/PMIA/PEO/LiTFSI CPEs

Poly (ethylene oxide) (PEO, MW= 600000) and lithium bistrifluoromethanesulfonimide (LiTFSI, 99.99%) are purchased commercially and are not further purified prior to use. PEO and LiTFSI and a certain amount of LBTO inorganic ceramic nanofibers were dissolved in anhydrous acetonitrile (CH_3CN) solution (molar ratio of [EO] to [Li] =12:1). After continuous mixing, the mixture was

evenly coated with glass rods on the surface and inside of two aramid oriented nanofiber films of the same size by a simple solution casting method. It is then dried in 50°C oven for 48 h to remove the residual solvent, and then the resulting composite solid electrolyte sample is transferred to glove box filled with argon gas for use.

1.4 Preparation of all-solid-state lithium batteries

The SSLMBs were assembled in CR2032 coin cells by contacting a lithium metal anode, the as-prepared electrolytes and a LiFePO$_4$ cathode. The cathode slurry was composed of 60 wt% LiFePO$_4$, 20 wt% PEO, 10 wt% LiTFSI and 10 wt% Super P added to anhydrous acetonitrile. After stirring for 48 h, it was coated on a carbon-coated aluminum foil and the acetonitrile solvent was removed under vacuum at 50 °C. Then, the electrode was punched into circular sheets with the same diameter as the electrolyte of 14 mm. The loading of the LiFePO$_4$ active material was approximately 1.5 mg cm^{-2}. The LiNi$_{0.8}$Co$_{0.1}$Mn$_{0.1}$O$_2$ (NCM) cathode was obtained by mixing the NCM, carbon black, polyvinylidene fluoride (PVDF) and LiTFSI (6:1:2:1 in mass ratio) in DMF solvents and then continuous stirring for 48 h. After that, the solution was coated on the carbon-coated aluminum foil and then transferred to a vacuum oven at 50 °C and dried for 48 h.

1.5 Material characterization

XRD analysis (XRD; BRUKER, D8 ADVANCE) was used to investigate the crystalline structure of LBTO NFs and LBTO/PMIA/PEO/LiTFSI films by scanning the angular range $5° \leq 2\theta \leq 80°$ using Cu Kα radiation ($\lambda = 1.5418$ Å). The morphology of precursor fiber membranes, PMIA NFs, LBTO NFs and electrolyte films was revealed by the field emission scanning electron microscope (FE-SEM; GeminiSEM 500) and the field emission high resolution transmission electron microscope (HR-TEM; JEM-F200) was used to analyze the interplanar spacing of LBTO NFs. The specific surface areas analysis of PMIA NFs and LBTO NFs was calculated using the Brunauer-Emmett-Teller (BET) method and the pore size distriution was synchronously carried out using the Barrett-Joyner-Halenda (BJH) method. Elemental mapping was conducted on an energy-dispersive X-ray spectroscopy (EDS; EDAX OCTANE SUPER). X-ray photoelectron spectroscopy (XPS) measurements were carried out using the NEXSA (NEXSA). The photoelectrochemical measurement was completed by a three electrode photoelectrochemical cell, in which Pt wire and Ag|AgCl were used as the counter electrode and reference electrode respectively.

Atomic force microscope (AFM) test was completed on Bruker Dimension ICON. The UV-vis absorbance spectra were obtained using a PE lambda 750 spectrophotometer. The Fourier transform infrared (FTIR) spectra were obtained on Thermo Fisher Nicolet iS50 FTIR spectrometer in the range of 4000-400 cm^{-1}. The thermal stability of electrolyte was analyzed on a STA 449F5 simultaneous thermal analysis under nitrogen atmosphere, where the temperature range was from 0 °C to 800 °C with the heating rate of 10 °C min^{-1}. The melting point and glass transition temperature were obtained by differential scanning calorimetry (DSC; NETZSCH, DSC200F3) which increased from -80 °C to 100 °C at a heating rate of 10 °C min^{-1} under a N$_2$ atmosphere. A YG005E monofilament tensile tester with the stretching speed set as 30 mm min^{-1} was used to measure the tensile shear property of the composite electrolyte. Considering the bidirectional network structure, CPEs is tested by taking the stretching direction of the Angle bisector.

1.6 Electrochemical measurements

All the electrochemical tests were carried out using the electrochemical workstation (CHI660E) and battery test system (LAND CT2001A).

The electrolyte with a diameter of 16 mm was sandwiched between two stainless steel electrodes (SS), and the σ of the electrolytes was measured by the EIS with the frequency range of 10^6 to 10^{-1} Hz between 30 and 70 °C. The σ values were obtained from **equation (1)**,

$$\sigma = \frac{L}{RS} \tag{1}$$

where L (cm) is the thickness of electrolyte film, and R (Ω) is the resistance value of the bulk electrolyte, and S (cm^2) is the electrode area.

The t^+ for the electrolyte films was measured by the direct-current (DC) polarization (with a DC voltage of 10 mV) and alternating-current (AC) impedance spectra (from 10^6 to 10^{-1}Hz) using two lithium metal anodes as the nonblocking electrodes at 50 °C. The t^+ values were measured and calculated according to the **equation (2)**

$$t^+ = \frac{I_{ss}(\Delta V - I_0 R_0)}{I_0(\Delta V - I_{ss} R_{SS})} \tag{2}$$

in which the ΔV, R_0 and R_{ss}, I_0 and I_{ss} represent the amplitude of applied polarization potential (10 mV), impendence value according to the EIS method before and after polarization, and initial and steady-state current, respectively. In addition, the

stripping/plating behavior of electrolyte films was measured using Li|CPEs|Li symmetric cells at different current densities at 50 °C.

To obtain the electrochemical stability window of electrolyte films, at 50 °C, the LSV of Li|CPEs|SS were conducted at a scan rate of 1 mV s^{-1} in a potential range of 2.1 and 5.5 V (vs Li$^+$/Li).

For the long cycle performance of cell with LiFePO$_4$ cathode, the charge and discharge performance were conducted under 50 °C at 0.5 C, and the voltage range was set between 2.8 V and 3.85 V. The rate performances from 0.1 C to 2 C of the cell were measured at 50 °C. For cell performance with NCM cathode at 50 °C, the voltage range was set between 2.8 V and 4.3 V.

1.7 DFT computation

All the DFT calculations were conducted based on the Vienna Ab-inito Simulation Package (VASP).[S2-3] The exchange-correlation effects were described by the Perdew-Burke-Ernzerhof (PBE) functional within the generalized gradient approximation (GGA) method.[S4-5] The core-valence interactions were accounted by the projected augmented wave (PAW) method.[S6-8] The energy cutoff for plane wave expansions was set to 450 eV. The structural optimization was completed for energy and force convergence set at 1.0×10^{-5} eV and 0.01 eV Å^{-1}, respectively. For the structural optimization, a $3 \times 2 \times 2$ supercell of LiBiTiO3 was employed with a vacuum layer thickness of 20 Å. The k-point mesh was set to $2 \times 3 \times 1$, with an energy convergence criterion of 1e-5 eV and a force convergence criterion of 0.01 eV/Å. The density of states (DOS) and work function calculations were performed using the optimized supercell and a k-point mesh of $4 \times 6 \times 2$. During the adsorption studies, the optimized supercell and TFSI were positioned at the appropriate adsorption sites and relaxed using a k-point mesh of $2 \times 3 \times 1$, with the same energy and force convergence criteria as mentioned above. Subsequent DOS and work function calculations for the adsorbed systems were conducted on the relaxed structures, using a k-point mesh of $4 \times 6 \times 1$. The work function (Φ) is defined:
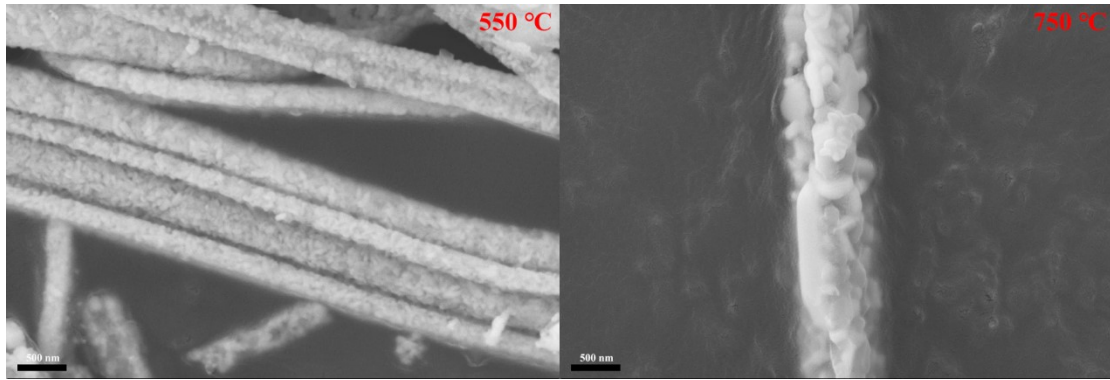
$$\Phi = E_{Vac} - E_F \tag{3}$$

where E_{Vac} is the electrostatic potential of the vacuum level and E_F is the Fermi energy.
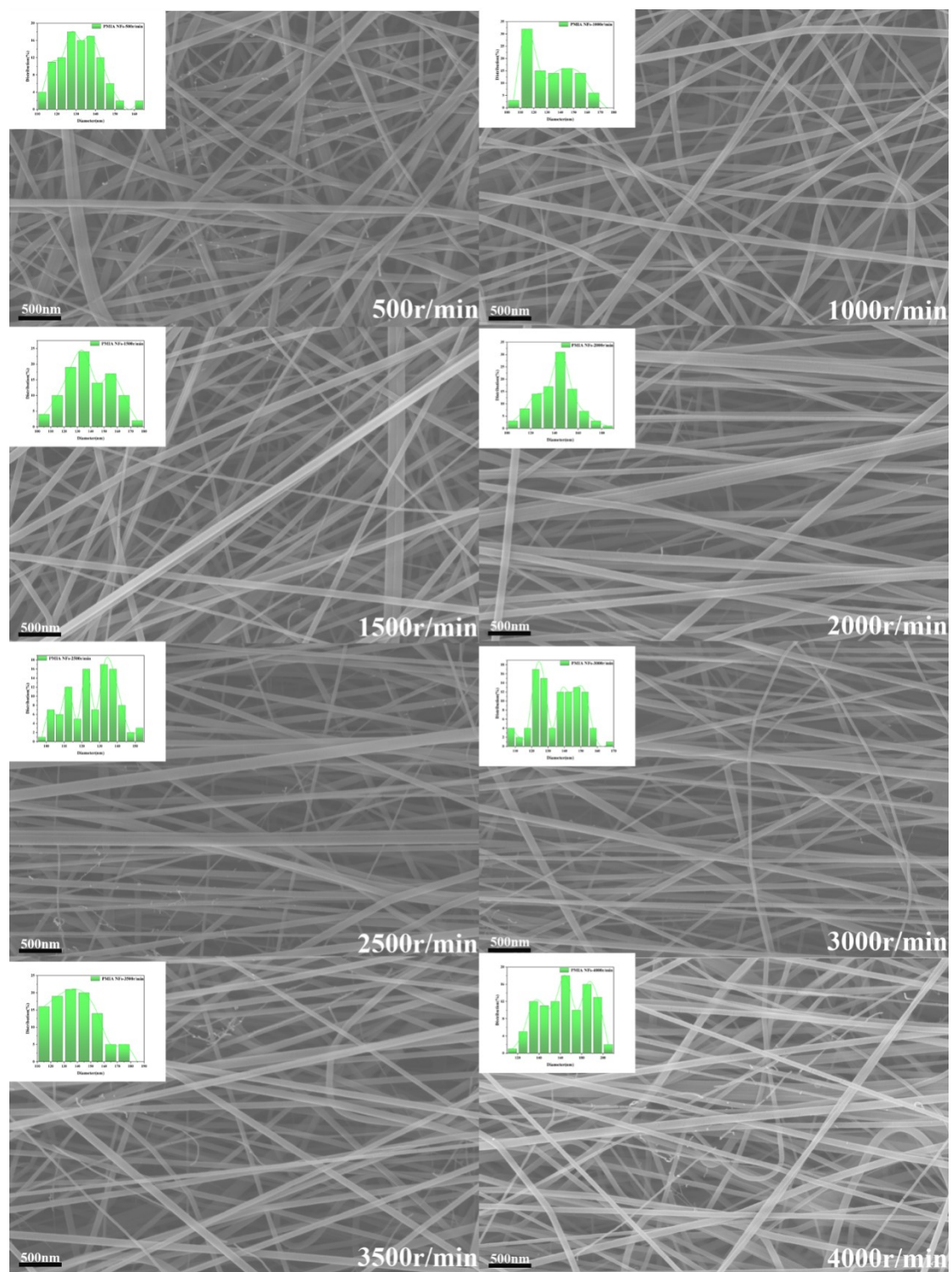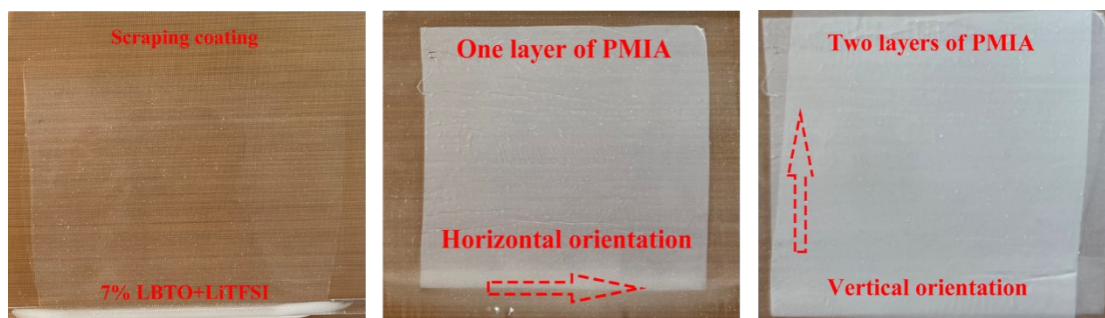
Figure S1 SEM images and fiber diameter distribution images of PMIA NFs under different rotational speed conditions.
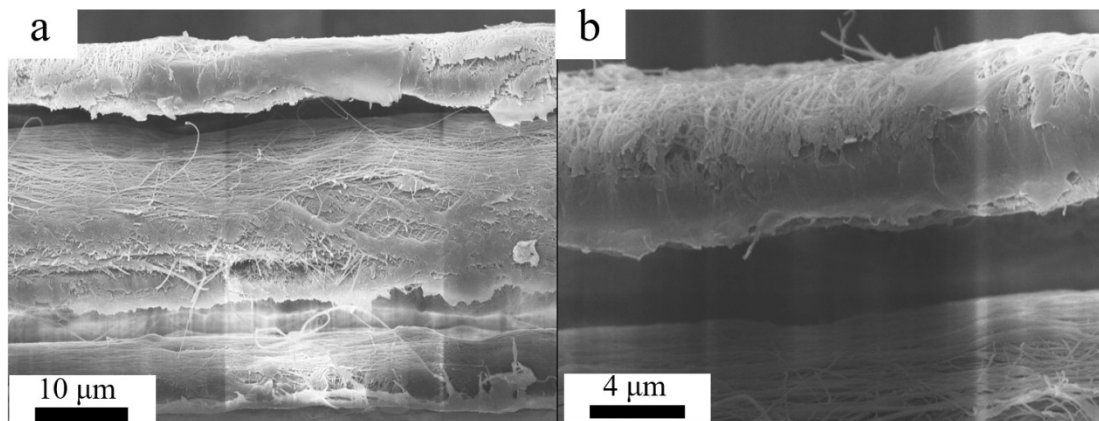
Figure S2 SEM images of LBTO NFs after calcination at 550℃ and 750℃ respectively.

**Figure S3** flow chart of CPEs preparation under physical objects.

Figure S4 (a) and (b) show the SEM images of the dual-oriented structure of PMIA fibers in the composite electrolyte at different magnifications.

As depicted in **Figure S4**, the electrolyte consists of two layers of mutually perpendicular PMIA nanofiber membranes. These two nanofiber membranes function as the skeletal support for the network-structured solid electrolyte, providing exceptional mechanical strength to the solid electrolyte.
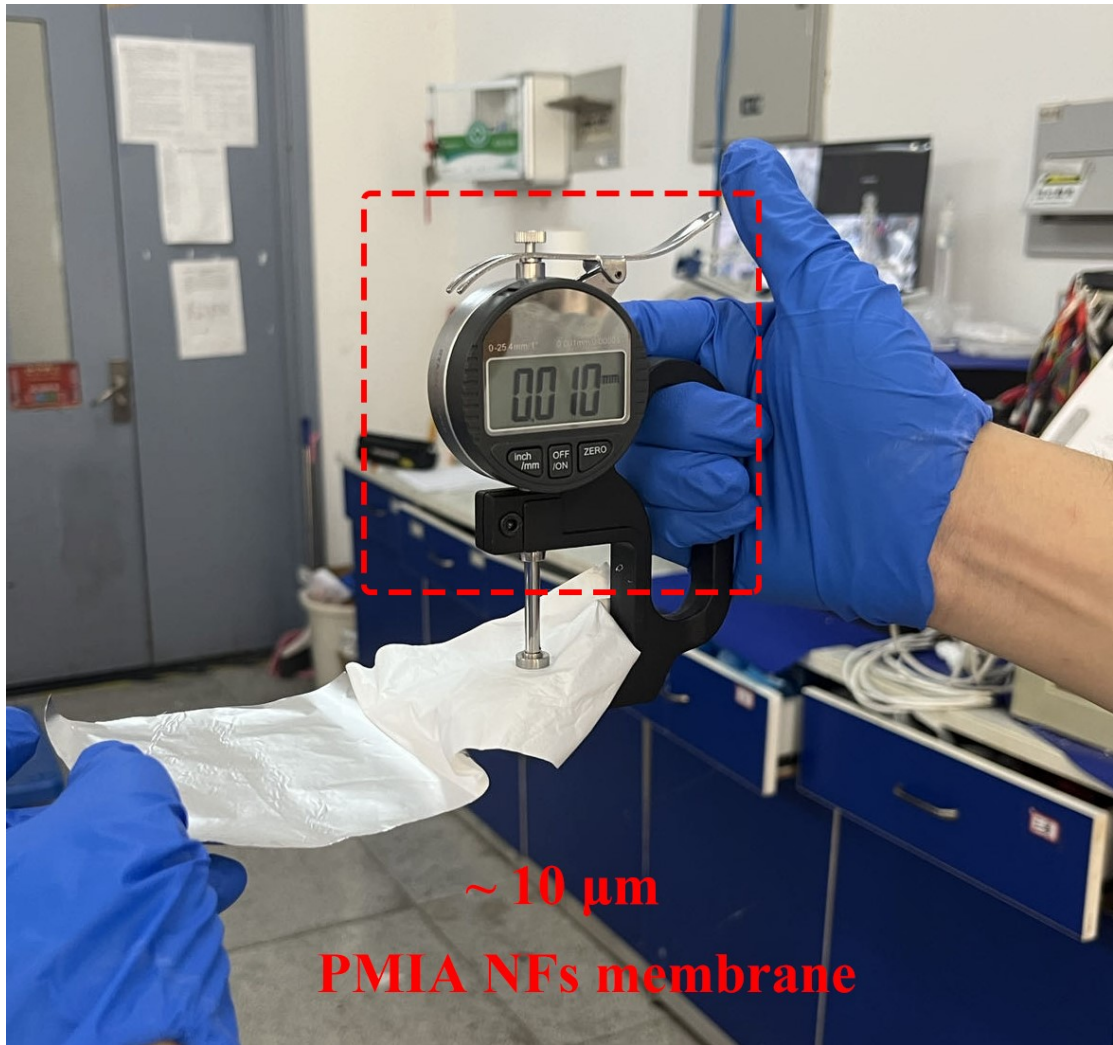
**Figure S5** Thickness measurements of PMIA nanofiber films at 2500 r/min.
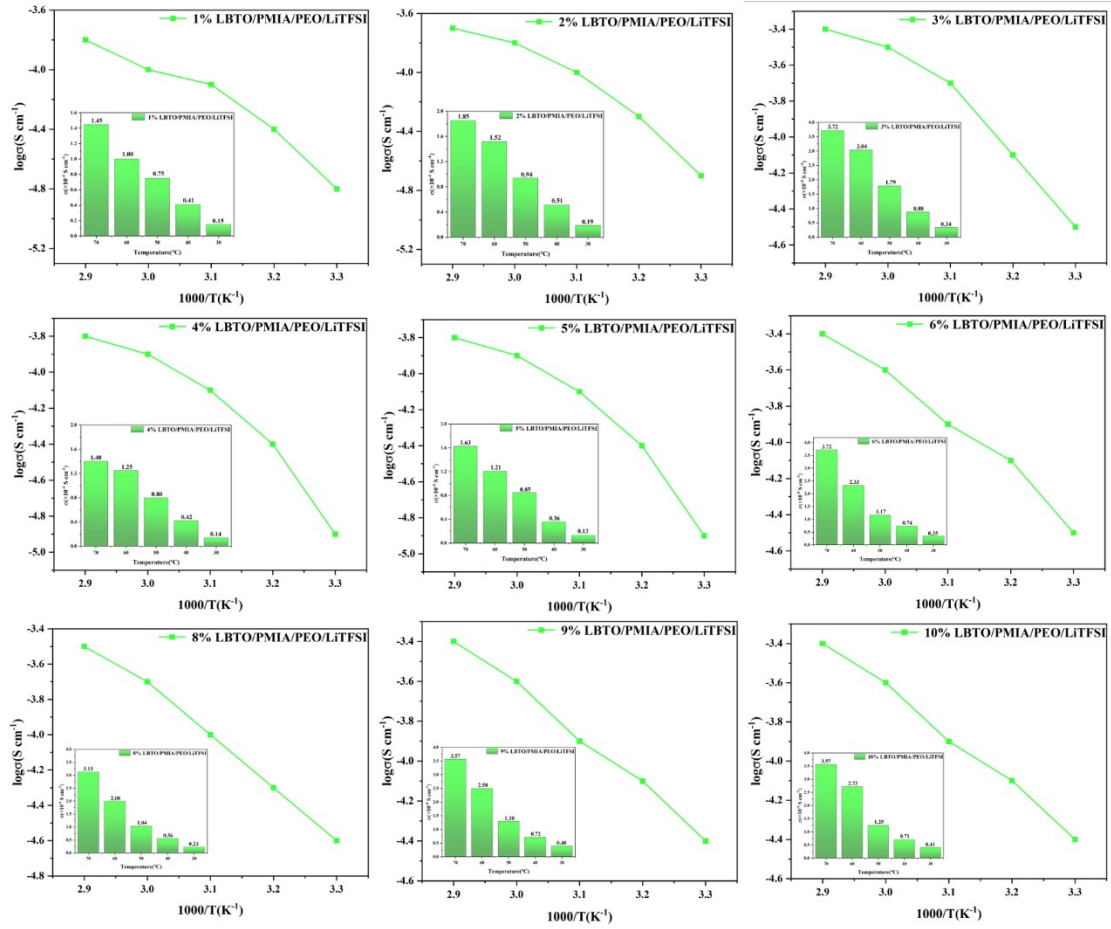
Figure S6 Arrhenius curve of CPEs under different LBTO additive content.
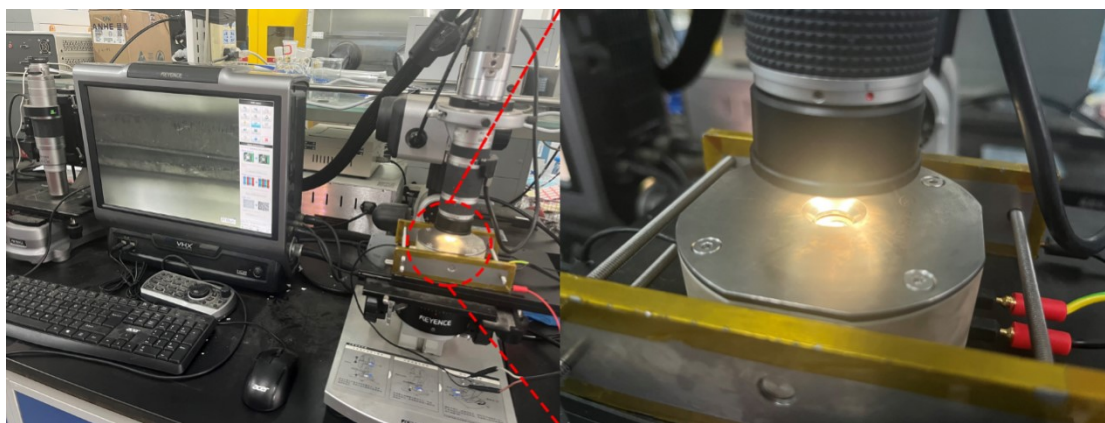
Figure S7 Li dendrite observation physical instrument image.

Table S1. Electrochemical properties of solid electrolyte with horizontal orientation structure.

| Oriented material	Ionic conductivity (S/cm)	Li ‖ Li cell	Strength	Refe
Q-COF	1.5×10^{-4} (60°C)	>1000 h	>10 GPa (Young's modulus)	[S1]
LLTO	4.67×10^{-4} (25°C)	>700 h	/	[S2]
LLZO	1.16×10^{-4} (30°C)	>700 h	1.8 MPa	[S3]
O-LLZO	/	9800 h	/	[S4]
OA-P-15C5	1.3×10^{-4} (25°C)	>1400 h	89.10 kPa	[S5]
LLISE	1.3×10^{-4} (30°C)	>1500 h	3.2 GPa (compressive strength)	[S6]
LAGP	1.6×10^{-4} (RT)	/	~20 Mpa (flexural failure strain)	[S7]
LAGP	1.25×10^{-4} (30°C)	>700 h	7.8 GPa (flexural modulus)	[S8]
ANF	5.5×10^{-5} (RT)	/	5.0 GPa (Young's modulus)	[S9]
LBTO/PMIA	4.17×10^{-4} (50°C)	>3000 h	20.45 MPa	This work
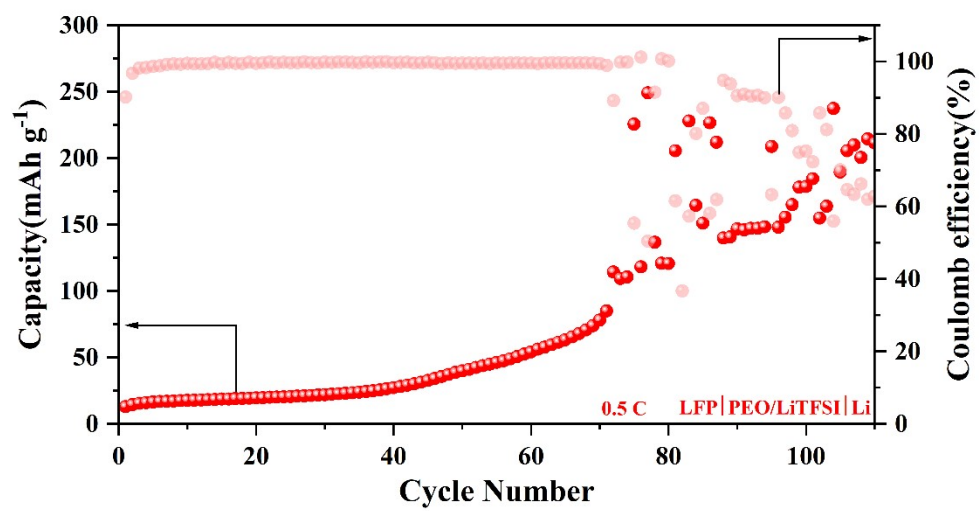
Figure S8 Long cycle test image of LFP-LMBs composed of PEO/LiTFSI CPEs at 50°C and 0.5 C current density.
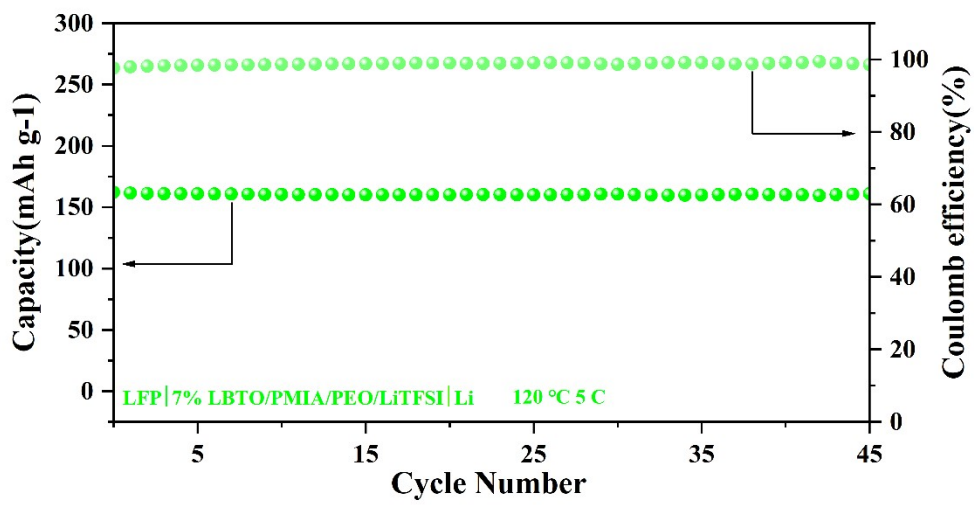
Figure S9 Charge and discharge cycle test diagram 7% LBTO/PMIA/PEO/LiTFSI CPEs at 120°C, 5 C.
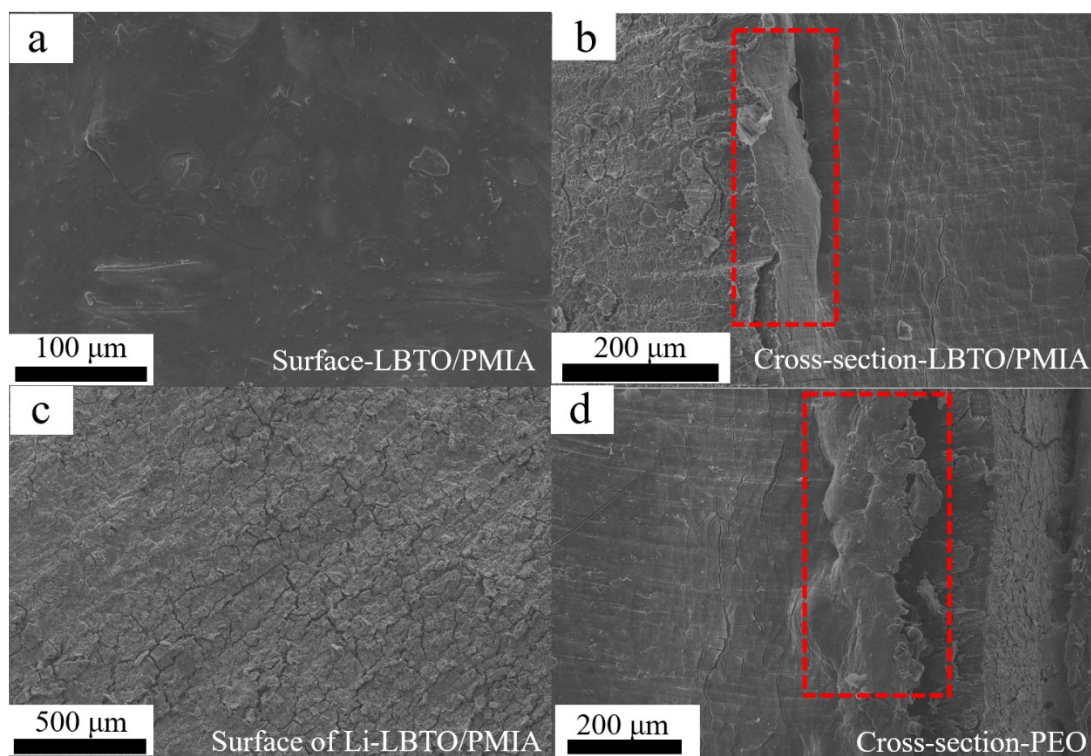
Figure S10 SEM images of (a) CSE-LBTO/PMIA surface, (b) CSE-LBTO/PMIA cross-section, (c) Li-LBTO/PMIA surface, and (d) CSE-PEO cross-section.

The studies have shown that Deng *et al* [S10] achieved remarkable mechanical flexibility and high ionic conductivity at room temperature by designing cross-linked network polymer electrolytes. And the related tests suggested that the formation of lithium dendrites can be effectively inhibited by mitigating the unevenness of local ion transport. Furthermore, PMIA possesses unique benzamide bonds that can engage in strong interactions with Li, thereby enhancing the transport of Li$^+$ [S11, S12]. **Figure S10** presents the SEM images of the electrolyte surface, cross-section and Li metal surface after battery cycling. As can be seen from **Figure S10(a)** and S**10(b)**, the prepared CSE-LBTO/PMIA, due to its excellent mechanical properties, is able to maintain a good morphology and relatively smooth surface after cycling. **Figure S10(c)** shows the surface image of the Li metal after cycling, with a relatively flat surface reflecting that the obtained CSE-LBTO/PMIA can reduce the negative effects caused by uneven Li deposition and effectively inhibit the formation of lithium dendrites. **Figure S10(d)** is the cross-sectional image of CSE-PEO after cycling, indicating that its poor mechanical properties limit its effectiveness in inhibiting lithium dendrites.

Reference

[S1] Niu C, Luo W, Dai C, et al. High-voltage-tolerant covalent organic framework electrolyte with holistically oriented channels for solid-state lithium metal batteries with nickel-rich cathodes[J]. Angewandte Chemie International Edition, 2021, 60(47): 24915-24923.

[S2] Li Y, Zhai Y, Xu S, et al. Using LLTO with vertically aligned and oriented structures to improve the ion conductivity of composite solid-state electrolytes[J]. Materials Today Communications, 2022, 33: 104243.

[S3] Zhao Y, Yan J, Cai W, et al. Elastic and well-aligned ceramic LLZO nanofiber based electrolytes for solid-state lithium batteries[J]. Energy Storage Materials, 2019, 23: 306-313.

[S4] Mu Y, Chu Y, Shi Y, et al. Constructing Robust LiF-Enriched Interfaces in High-Voltage Solid-State Lithium Batteries Utilizing Tailored Oriented Ceramic Fiber Electrolytes[J]. Advanced Energy Materials, 2024: 2400725.

[S5] Zhao Y, Gao M, Qin Y, et al. Electric field induced molecular orientation to construct the composite polymer electrolytes with vertically aligned ion diffusion pathways for stable solid-state lithium metal batteries[J]. Chemical Engineering Journal, 2024, 495: 153645.

[S6] Guo S, Kou W, Wu W, et al. Thin laminar inorganic solid electrolyte with high ionic conductance towards high-performance all-solid-state lithium battery[J]. Chemical Engineering Journal, 2022, 427: 131948.

[S7] Zekoll S, Marriner-Edwards C, Hekselman A K O, et al. Hybrid electrolytes with 3D bicontinuous ordered ceramic and polymer microchannels for all-solid-state batteries[J]. Energy & Environmental Science, 2018, 11(1): 185-201.

[S8] Li A, Liao X, Zhang H, et al. Nacre-inspired composite electrolytes for load-bearing solid-state lithium-metal batteries[J]. Advanced Materials, 2020, 32(2): 1905517.

[S9] Tung S O, Ho S, Yang M, et al. A dendrite-suppressing composite ion conductor from aramid nanofibres[J]. Nature communications, 2015, 6(1): 6152.

[S10] Wen S, Luo C, Wang Q, et al. Integrated design of ultrathin crosslinked network polymer electrolytes for flexible and stable all-solid-state lithium batteries[J]. Energy Storage Materials, 2022, 47: 453-461.

[S11] Luo S, Deng N, Wang H, et al. Facilitating Li^+ conduction channels and suppressing lithium dendrites by introducing Zn-based MOFs in composite electrolyte membrane with excellent

thermal stability for solid-state lithium metal batteries[J]. Chemical Engineering Journal, 2023, 474: 145683.

[S12] Xiang H, Gao L, Shi D, et al. Fast Ion Conductor Nanofibers and Aramid Nanofibers with Hydrogen Bonds Synergistically Enhanced Composite Solid Electrolytes[J]. Advanced Fiber Materials, 2024, 6(3): 883-899.